Natural payload delivery of the doxorubicin anticancer drug from boron nitride oxide nanosheets

E. Duverger, Sebastien Balme, Mikhael. Bechelany, Philippe Miele, F. Picaud

Natural Payload Delivery of the Doxorubicin Anticancer Drug from Boron Nitride Oxide Nanosheets

E. Duverger[a], S. Balme[b], M. Bechelany[b], P. Miele[b] and F. Picaud[c,].*

[a] *FEMTO-ST Institute, Université Bourgogne Franche-Comté, CNRS, 15B avenue des Montboucons, F-25030 Besançon, Cedex, France*

[b] *Institut Européen des Membranes, IEM – UMR 5635, ENSCM, CNRS, Univ Montpellier, Montpellier, France*

[c] *Laboratoire de Nanomédecine, Imagerie et Thérapeutique, Université Bourgogne Franche-Comté (UFR Sciences et Techniques), EA 4662, Centre Hospitalier Universitaire de Besançon, 16 route de Gray, 25030 Besançon, France*

*Corresponding author: fabien.picaud@univ-fcomte.fr

ABSTRACT

We studied the behavior of doxorubicin (DOX; an anticancer drug) molecules loaded on a boron nitride oxide nanosheet (BNO-NS) using the density functional theory (DFT), time-dependent density functional theory (TDDFT), and molecular dynamic (MD) simulation methods. We found that DOX molecules in interaction with BNO-NS preserve their optical properties in water. Moreover, the BNO-NS vector allowed stabilizing the DOX molecules on a cellular membrane. From these results, we conclude that BNO-NS represents a good

candidate for DOX molecule transport and stabilization near a cell membrane for longer time compared with isolated DOX molecules that tend to be repulsed by the membrane. In this drug delivery system, the choice of BNO-NS as nanovector is important because it allows delivering an elevated therapeutic dose directly on the cancer cell target.

Keywords: boron nitride oxide nanosheets, therapeutic agents, time-dependent density functional theory, molecular dynamics

1. INTRODUCTION

Nanobiotechnology research has promoted the emergence of new anti-cancer strategies thanks to the development of various types of nanovectors, such as quantum dots, dendrimers, nanotubes, gold (and silver) nanoparticles, liposomes and micelles. Nanomedicine breakthroughs depend on the capacity of designing and producing well-defined nanosystems with suitable physicochemical properties and biological effects. [1-6]

Among the different nanosystems, the biomedical applications of carbon and boron nitride (BN)-based materials, including for drug delivery, have grown rapidly in the past few years. [7-11] New nanostructures are now in development, such as graphene and BN 2D nanosheets (BN-NS) for future applications in medicine, thanks to the progress in liquid-phase exfoliation that is now scaled up for industrial production.[12, 13] The synthesis of graphene and hexagonal BN has favored theoretical and experimental studies on these classes of materials that are suitable for many different applications.[14, 15] Graphene is a zero band gap semi-metal, whereas the BN sheet is an insulator in which the B–N bonds display a partial ionic character.[16-19] Moreover, covalent functionalization of graphene and BN is

now possible to increase their solubility in physiological solutions, thanks to the presence of epoxy (-O) and hydroxyl groups (-OH) on their surface, and also to enhance their immune biocompatibility and to reduce significantly their toxicity.[20-24]. Therefore, these materials are currently studied for the design of advanced delivery systems for a broad range of therapeutics, such as doxorubicin (DOX).

DOX is one of the main chemotherapeutic agents for the treatment of leukemia, invasive transitional cell carcinoma of the bladder, and other solid cancers. [4, 25, 26] However, its use is limited by the many side effects (e.g., hair loss, nausea and vomiting, and heart damage) and poor pharmacokinetics (rapid decrease in plasma). To circumvent such limitations and also to reduce the side effects, promising alternative administration strategies have been recently proposed by using drug delivery vehicles [26-29], such as hydroxylated BN (i.e., BN oxide nanosheets, BNO-NS). These studies have demonstrated that hydroxylated BN improve DOX solubility and payload. In this conformation, BNO-NS could adsorb up to 309% of its weight in DOX. Moreover, this drug-loaded vehicle also exhibited pH-dependent release kinetics. Specifically, at acidic pH, DOX was released in higher amounts and at higher rates and cancer cell viability was reduced to 21%. [10, 21]

The adsorption of a chemotherapeutic drug onto a delivery vehicle and the determination of its properties (energy affinity, bonding, optical properties …) need to be determined to improve our knowledge on such drug delivery systems. Here, we used simulation methods to study the adsorption of DOX on BNO-NS in vacuum and also in the presence of water. In the first part of this paper, we report the density functional theory (DFT) results concerning DOX adsorption on the BNO-NS surface in vacuum. We found that DOX was spontaneously adsorbed on this nanostructure. Then, we determined the conditions for DOX physisorption and chemisorption and the consequent energy stability. We obtained additional information on the photodynamic properties of the DOX/BNO-NS system using

time dependent density functional theory (TDDFT) calculations in water. We then compared the TDDFT data with experimental results to validate the type of preferential DOX adsorption onto BNO-NS. In the second part, we performed molecular dynamics (MD) simulations, based on the DFT preliminary results, in a full biological environment to obtain insights on the stability of the DOX/BNO-NS system in water with NaCl ions and in the presence of a cell membrane. This method allowed us to demonstrate that this system could be used to increase DOX concentration on cancer cells.

2. EXPERIMENTAL

2.1 Synthesis

2.1.1. Preparation of BNO-NS

Exfoliated and hydroxylated BN was prepared according to a previously described procedure.[14, 30] To prepare the gelatin solution (20% in mass ratio), gelatin powder (Sigma Aldrich) was dissolved by magnetic stirring in distilled water at 60°C for 1h. BN powder (H.C. Starck) was then added to the gelatin solution (mass ratio of 1/20 BN/gelatin). The mixture was treated (sonicated?) with an ultrasonic probe system (SONOPULS HD 3100) for 1h (60% amplitude and pulse on/off for 1 second). After centrifugation at 3000 rpm for 1h, the supernatant (i.e., the stable gelatin/BN dispersion containing the exfoliated BN) was dried at 80°C for 24h and heated at 650°C for 4h to eliminate the gelatin from the solution. The obtained exfoliated and hydroxylated BN was fully characterized using X-ray diffraction, Raman spectroscopy, atomic force microscopy, Brunauer–Emmett–Teller surface area analysis, and transmission and scanning electron microscopy. The characterization results were previously reported.[31] This analysis confirmed the formation of BN nanosheets with a thickness of 2 nm and consisting of several BN layers.

2.1.2 Preparation of DOX/BNO-NS

DOX/BNO-NS was prepared by mixing the BNO-NS suspension (C = 1 mg ml^{-1}) with DOX (C = 4 10^{-5} mol l^{-1}) in water for 10min. Then, the mixture was dialyzed to remove unloaded DOX.

2.2 Characterization

The UV–Vis absorption spectra of DOX and DOX/BNO-NS samples dispersed in water were obtained using a Vis/NIR spectrometer. DOX showed a bump around 280 nm and an adsorption in the visible light between 400 and 550 nm. DOX/BNO-NS displayed a bump at around 300 nm and an adsorption in the visible light between 420 and 700 nm (Fig. 1). Many previous studies reported that BN-NS (BNO-NS?) has an absorption peak at around 200 nm, which is the characteristic peak of the band gap for BN, and a small bump around 250 nm, which could be caused by the presence of vacancy defects in the NS crystal structure (not shown).[32-34]

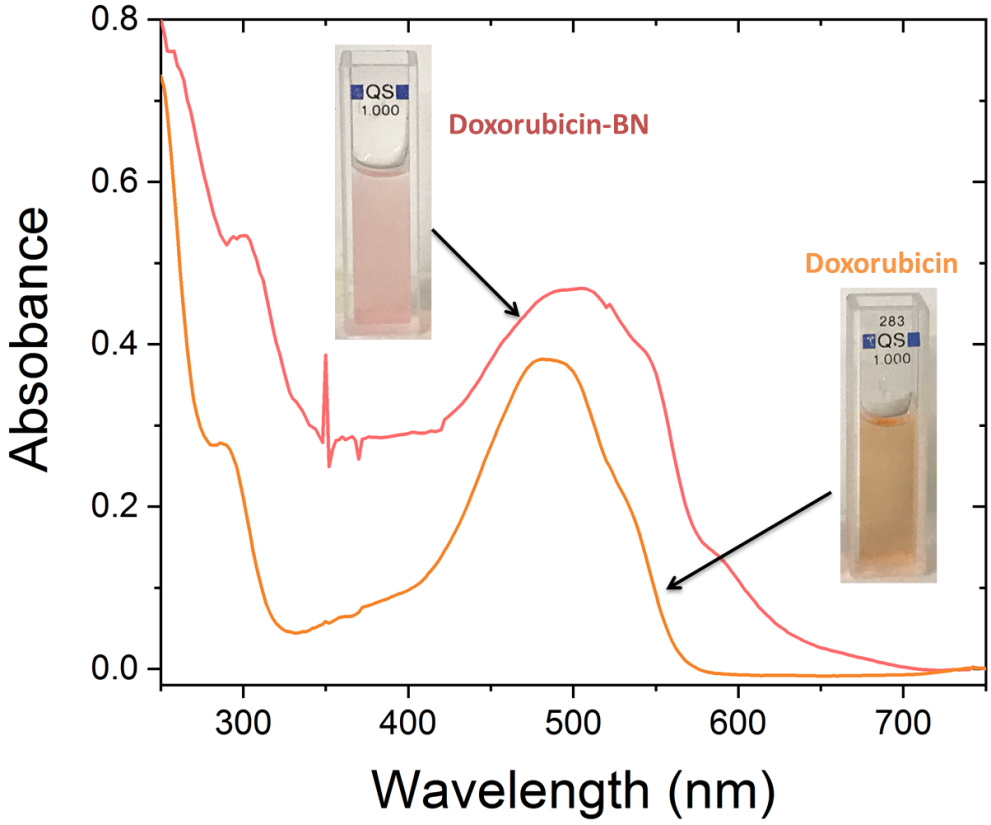

Figure 1. UV-Vis spectra of DOX and DOX/BNO-NS in water. In figure I would use DOX and DOX/BNO-NS.

3. MODELS AND THEORETICAL DETAILS

DOX adsorption onto the BNO-NS surface was evaluated using the periodic Kohn-Sham DFT calculations for periodic systems and the SIESTA program.[35, 36] The Perdew–Burke–Ernzerhof (PBE) Generalized Gradient Approximation (GGA) for the exchange-correlation density functionals (implemented in the SIESTA package) was employed to determine the total energies.[37, 38] All calculations were performed without spin polarization, and with the following parameters: self-consistency mixing rate of 0.1, maximum force tolerance of 0.02eV.$Å^{-1}$, and mesh cut off of 200 Ry. The variations of these parameters showed a perturbation of the total adsorption energies lower than 0.1% (i.e., at

most $4x10^{-3}$ eV for a cut off of 300 Ry). The self-consistent cycles were stopped when the variations of the total energy per unit cell and the band structure energy were both lower than 10^{-4} eV. As large unit cells were used in all calculations (i.e., 80x80x80 $Å^3$), the Brillouin zone integration was reduced to a single k-point at the center Γ. Two cases were envisaged for DOX (Fig. 2). The first one (DOX1) considered the complete molecule with its NH_2 termination ($NO_{11}H_{29}C_{27}$) and constituted of 68 atoms. In the second one (DOX2), the DOX molecule contained only 67 atoms because one H atom was removed from the NH_2 end ($NO_{11}H_{28}C_{27}$) to take into account the molecule modification upon chemisorption. A basis set of localized atomic orbitals (double-ζ and polarization functions) and norm-conserving pseudopotentials was employed. After energetic optimization, BNO-NS (i.e., 134 atoms) included 38 N atoms and 38 B atoms, 12 hydroxyl radicals (-OH) and 10 epoxy groups (O) grafted on some of the B and N atoms, and hydrogen atoms on other dangling bonds to avoid boundary effects. Indeed, previous studies reported that hydroxyl (−OH) functional groups can be introduced onto BN-NS basal plane or edges.[39-42] Its lateral size was 16.95x13.40 $Å^2$. In the optimized BNO-NS molecule, the calculated average lengths of B-N bonds were around 1.44 Å, of hydroxyl B bonds around 1.48 Å, of hydroxyl N bonds around 1.48 Å, and of epoxy N and epoxy B bonds around 1.53 Å and 1.46 Å, respectively.

a)	b)

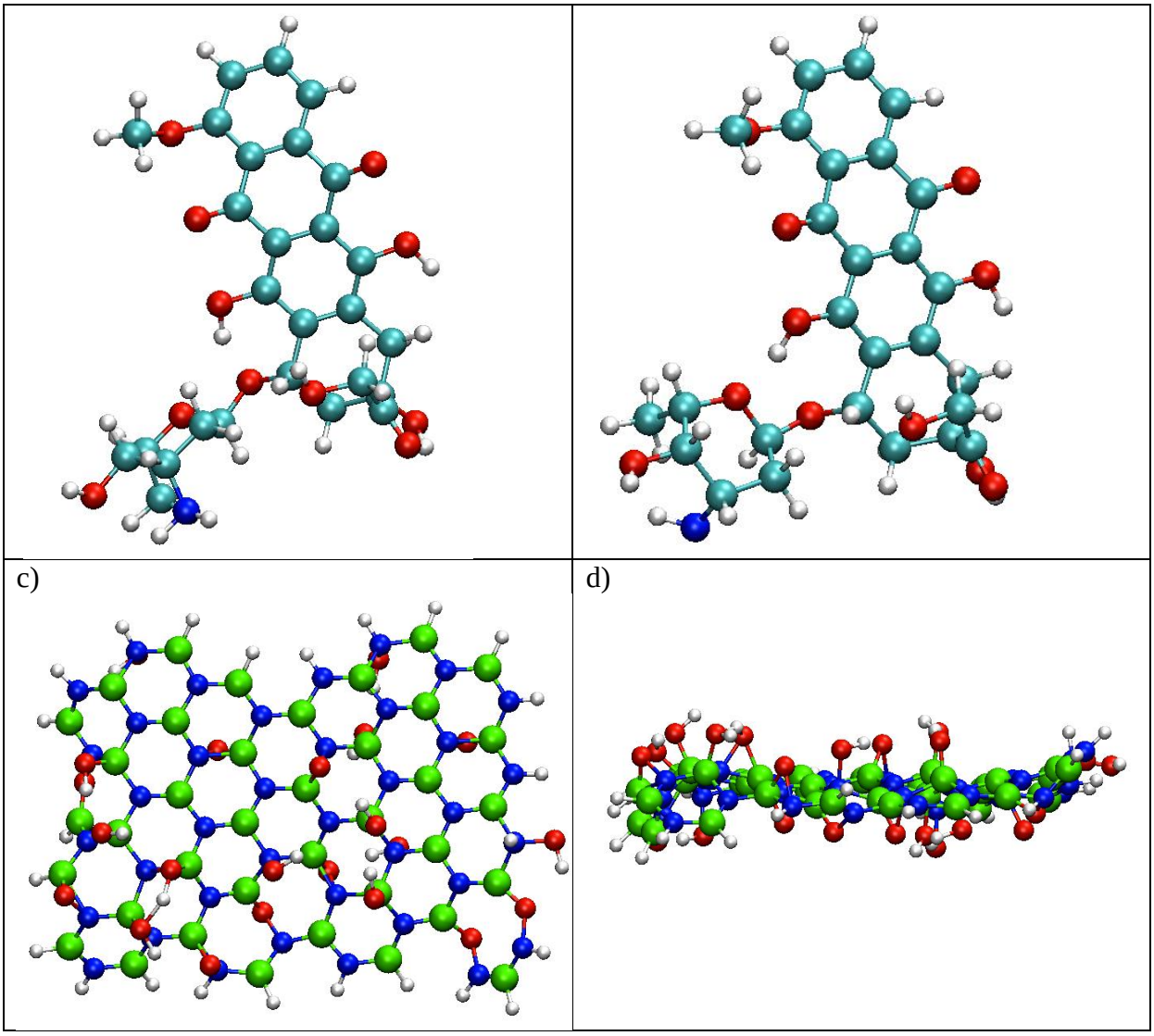

Figure 2. (a) DOX molecule with the NH_2 end (DOX1); (b) DOX molecule with the NH end (DOX2); (c) Top view and (d) Lateral view of BNO-NS (B, N, C, O, and H atoms are represented as green, blue, cyan, red, and white spheres, respectively).

To understand the DOX/BNO-NS interactions, the adsorption energy (Eads) of the adsorbed molecules (MOL) was defined as: $E_{ads} = E_{(MOL + BNO\text{-}NS)} - E_{(BNO\text{-}NS)} - E_{(MOL)}$. A negative Eads value indicates a more favorable interaction between the drug and the NS surface.

Here, the van der Waals interactions were not taken into account (although they could be preponderant during physisorption) to avoid unrealistic parameter calibration in the DFT model. Two different DOX orientations were investigated: parallel for DOX1 physisorption to

improve the π−π interactions, and perpendicular for DOX2 to favor the chemical cycloaddition reaction.

The charge repartition between DOX molecules and the BNO-NS surface was analyzed using a partial-charge approach (i.e., valence electrons) based on the Bader partitioning scheme.[43, 44] Then, to determine the best conformation of DOX1 and DOX2 on a BNO-NS, the absorption spectra in water were quantified using the TDDFT code developed in the Octopus package that generates different shape configurations to integrate the three space dimensions.[45-47] To calculate the different linear response spectra in the linear-response regime for DOX1, DOX2 and BNO-NS alone and for DOX/BNO-NS, the system was excited with the same infinitesimal electric-field pulse, and then the time-dependent Kohn−Sham equations was propagated for the same time, giving 4500 time steps (i.e., total time of 10.00 hbar/eV or 6.58fs). To propagate these wave functions, the energy was converged to 10^{-7} eV and the density to 10^{-6}. The spectra were then calculated by using the approximately enforced time-reversal symmetry for the TDDFT simulation with polarizable continuum model (PCM) simulations. The PCM method allows defining a solvent (in our case water) as a continuous dielectric medium polarized by the solute molecule.

MD simulations were performed by building the DOX molecular force field with the Force Field Toolkit package of the Visual Molecular Dynamics program.[48] The systems were solvated in a water box large enough to prevent the interaction of BNO-NS, DOX1 and DOX2 with their neighbors in the adjacent cell when periodic boundary conditions were used. NaCl ions (at a concentration of 0.15M) were added to the water model (transferable intramolecular potential with 3 points, TIP3P) to reproduce the correct biological environment. To mimic a cell environment, a cell membrane was built using 176 molecules of the glycerophospholipid 1-palmitoyl-2-oleoyl-sn-glycero-3-phosphocholine (POPC) and the protocol described in the CHARMM-GUI web site. This membrane was progressively

equilibrated using MD simulations (NAMD 2.12 package) for 50 ns.[49]. CHARMM36 force-field optimization parameters were used in all simulations.[50] During the simulations, the system temperature and pressure were kept constant at 310 K (Langevin dynamics) and 1 atm (Langevin piston), respectively. The long range electrostatic forces were evaluated using the classical particle mesh Ewald (PME) method with a grid spacing of 1.2 Å, and a fourth-order spline interpolation. The integration time step was equal to 1fs. Each simulation employed periodic boundary conditions in the three directions of space. During the MD simulations, all atoms were allowed to relax and water molecules could move freely in the simulation box. Each simulation was repeated at least three times to confirm the energy calculations. The electrical charges on each DOX1 and DOX2 atom were calculated using the equilibrium structures obtained with the DFT in the Bader scheme analysis.

4. RESULTS

4.1. Density Functional Theory

Geometry optimization of isolated DOX1 and DOX2 molecules and of BNO-NS alone (Fig. 2) showed that BNO-NS presented some distortions to accommodate hydroxyl and epoxy groups.

Then, to study the adsorption of DOX molecules on BNO-NS, a distance of 1.5 Å between the BNO-NS surface and the DOX molecules was selected before optimization of the whole system. All simulations on top of the epoxy and hydroxyl groups did not allow grafting the DOX2 molecule on the BNO-NS surface. The adsorption energy (Eads) of the interacting systems (DOX/BNO-NS) (Fig. 3) and the optimized distances between atoms of the DOX molecule (taken as the reference for the interacting system) and of the BNO-NS surface were also deduced from the simulations (Table 1).

a)

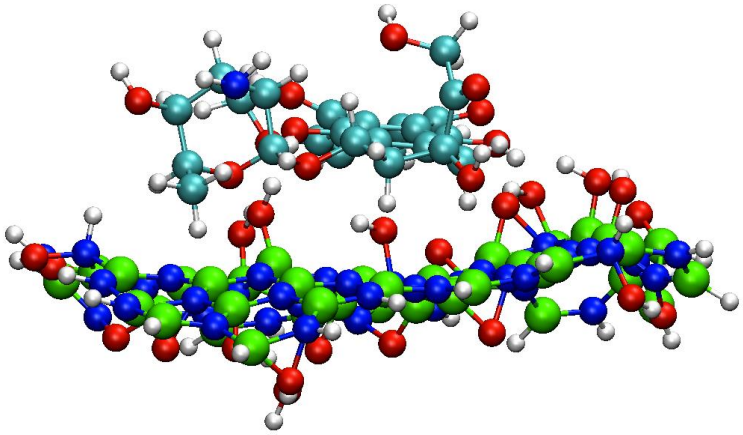

b)

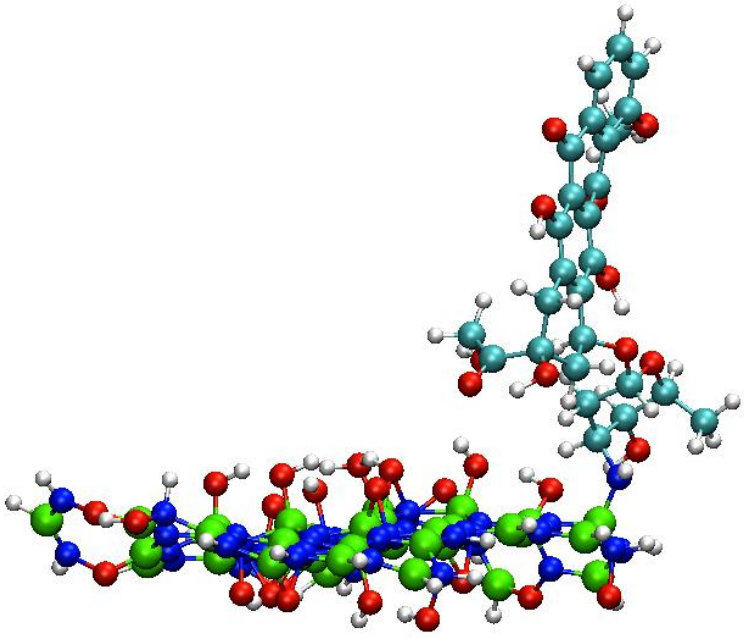

c)

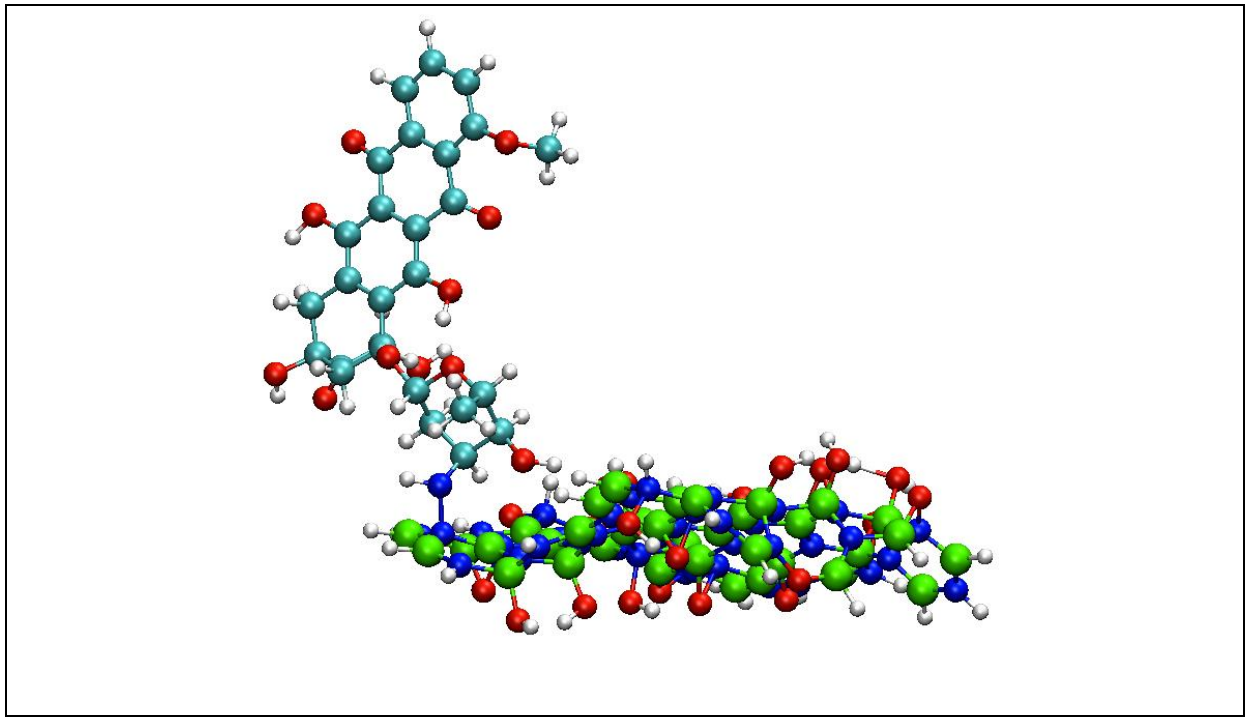

Figure 3. (a) Doxorubicin (DOX1) in π–π interaction with BNO-NS, (b) Boron bonding of DOX2 with BNO-NS, (c) Nitrogen bonding of DOX2 with BNO-NS (B, N, C, O, and H atoms are represented as green, blue, cyan, red, and white spheres, respectively). The DOX1 molecule was placed parallel to the BNO-NS surface to study physisorption, whereas the DOX2 molecule was presented perpendicular to the BNO-NS with its NH group on the top of N or B atoms for modeling chemisorption.

	DOX1 physisorption	DOX2 chemisorption	
	Parallel to BNO-NS	On B atoms	On N atoms
Eads (eV)	-1.48	-5.1	-3.28
Distance DOX/BNO-NS (Å)	3.53	1.51 (B-N)	1.53 (N-N)

Table 1: Distance and adsorption energy of DOX1 and DOX2 on BNO-NS.

Our results clearly showed that DOX1 physisorption onto BNO-NS was strong, although the van der Waals interactions were not taken into account (E_{ads}=-1.48 eV, distance DOX1/BNO-NS=3.53 Å). The Bader charge difference for the DOX1 molecule between the final state (adsorbed on the BNO-NS surface) and the initial state (isolated DOX1) was only 0.025 e^{-}.

For chemisorption, bending of the plane allowed lifting the sp^2 character of the BNO-NS surface. This facilitated the creation of bonds between the BNO-NS surface and the DOX2 molecule. The adsorption energy was low: -5.1 eV for the formation of one B–N bond of a length of 1.51 Å with the BNO-NS surface, and -3.28 eV for the formation of one N-N bond of a length of 1.53 Å. The Bader charge difference was 0.016 e^- when DOX2 was bonded to a B atom of BNO-NS, and -0.039 e- when bonded to an N atom of BNO-NS.

Then, the Octopus code was used to investigate the UV-vis absorption spectra of isolated DOX1 and DOX2 molecules (Fig. 4a) and BNO-NS alone (Fig. 4b), and of the DOX/BNO-NS systems (Fig. 4c-d). All these calculations were performed in a solvent fluid that mimics the dielectric water properties within the PCM model. The DOX features obtained by UV-vis spectrometry (Fig. 1) were present also in the DOX1 theoretical spectrum (Fig. 4a), with a band around 270 nm (280 nm experimentally) attributed in the literature to the $n -> \pi*$ transition, and a large absorbance band centered around 500 nm (480 nm experimentally) attributed to the $\pi -> \pi*$ transition in the DOX1 molecule.[51] Comparison of the DOX1 (mauve) and DOX2 (orange) theoretical spectra (Fig. 4a) showed only a blue shift displacement of the DOX2 spectrum of around 15 nm due to the NH radical, while the general shape of the absorbance curves remained the same for the two molecules. Therefore, one could hypothesize that DOX was dispersed experimentally in water in its pristine form. The theoretical BNO-NS spectrum (Fig. 4b) showed a bump around 250-300 nm that could be caused by the presence of vacancy defects in the NS crystal structure.[32-34] Moreover, a monotonic decrease of the absorbance was observed in the range of 300 nm to 750 nm. It is of particular interest to study the UV−vis response spectra to DOX adsorption on BNO-NS because they cannot be masked by the nanovector response spectrum. Compared with isolated DOX1 (blue) in water, DOX1/BNO-NS in π–π interaction (green) (Fig. 4c) showed a smaller bump in the absorbance peak around 270 nm due to the $n -> \pi*$ transition, and a larger, but

weaker in intensity absorbance bump centered on 550 nm. Comparison of the theoretical spectra of the DOX2 molecule alone (blue) and chemisorbed onto BNO-NS (on a B atom, the most favorable case) (red) (Fig. 4d) showed a red shift of the spectrum with the bump displaced at around 280 nm (n–> π* transition) and another bump (π –> π* transition) centered on 520 nm. This bump was more intense than in the case of DOX1 physisorbed on the BNO-NS surface. All the theoretical features mimicked adequately the absorbance spectrum results obtained experimentally by UV-vis spectrometry (Fig. 1). These data confirmed the good adsorption (physisorption and chemisorption) of DOX on the BNO-NS surface, suggesting that the system could be used for DOX delivery to cancer cells. The choice between physisorption and chemisorption will probably depend on the solvent.

a)

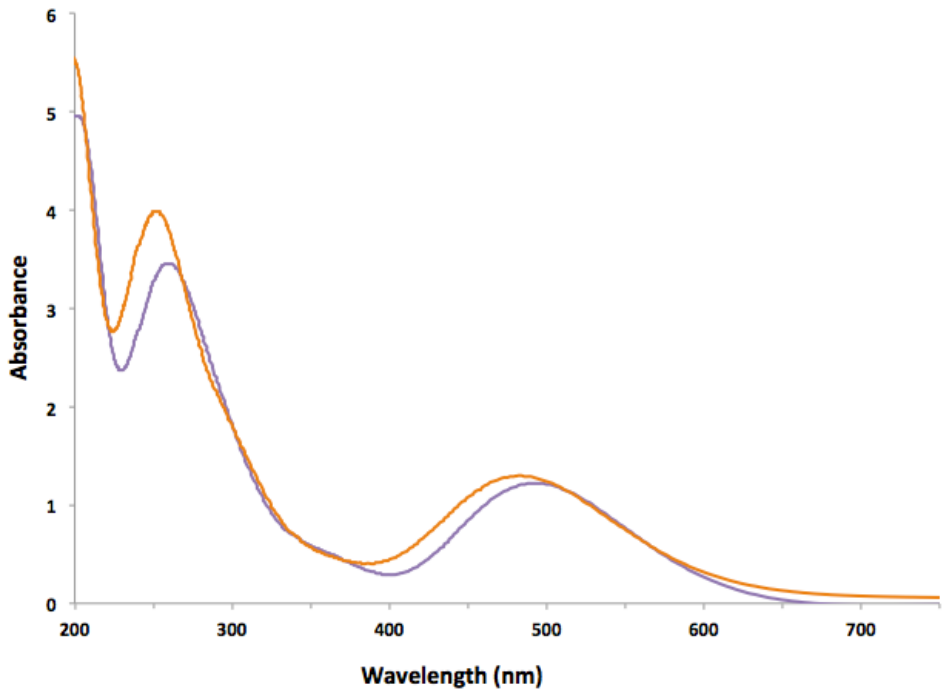

b)

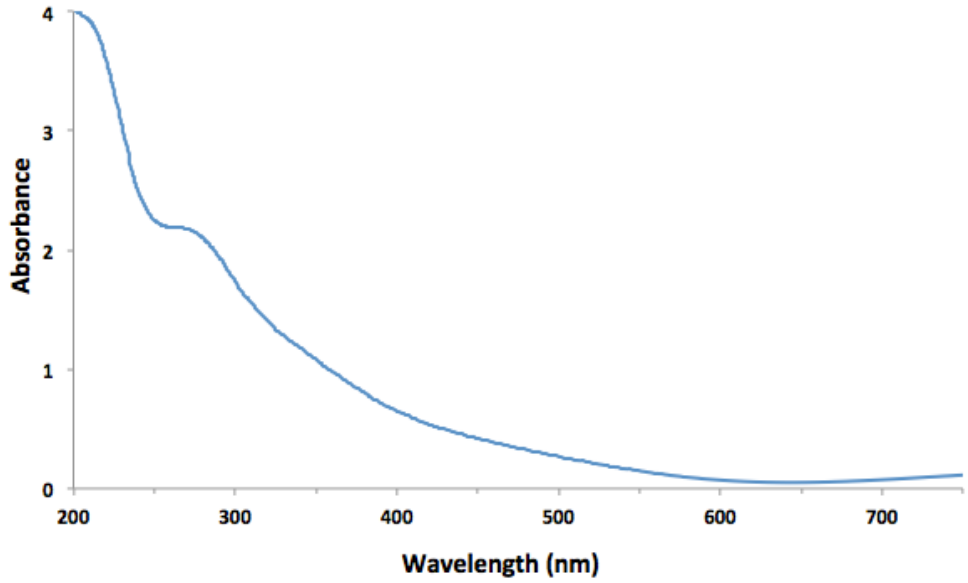
Absorbance
4
3
2
1
0
200
300
400
500
600
700
Wavelength (nm)

c)

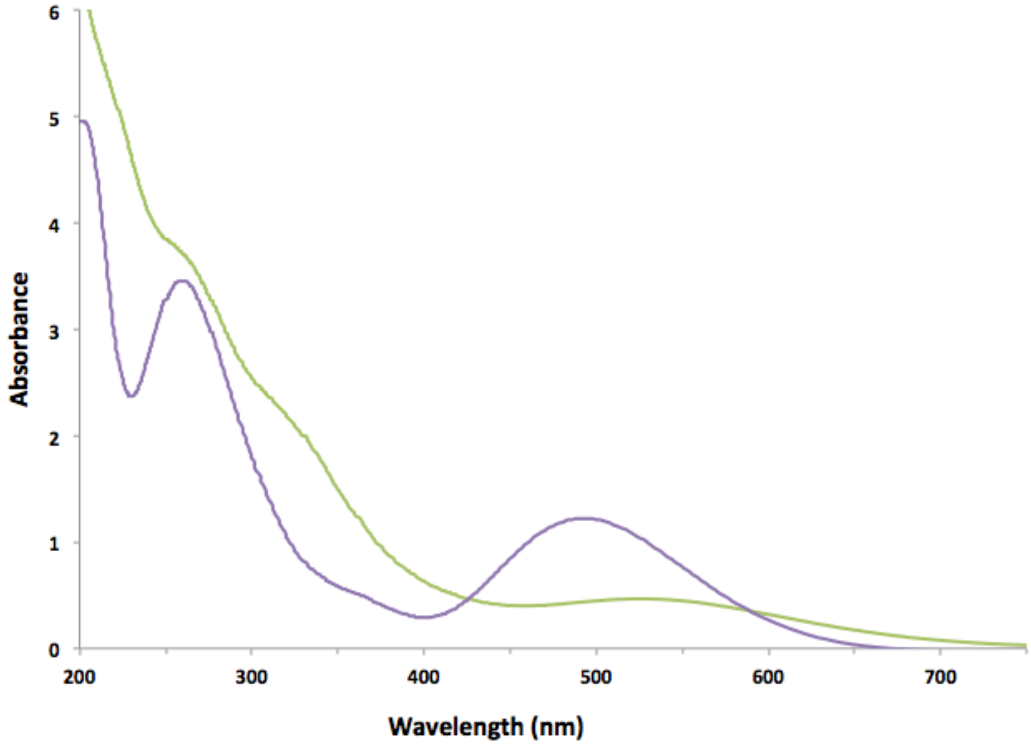
Absorbance
6
5
4
3
2
1
0
200
300
400
500
600
700
Wavelength (nm)

d)

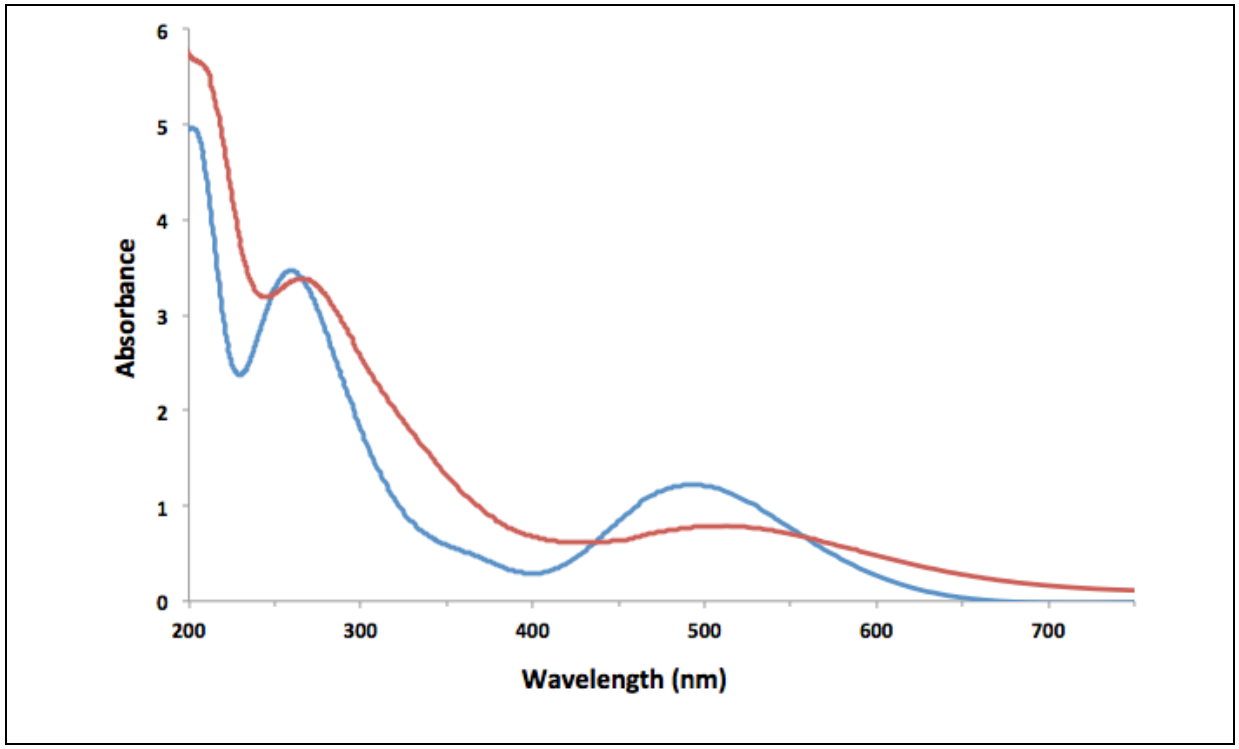

Figure 4. UV−vis absorption spectra (singlet states) obtained with PCM implemented in the Octopus code: (a) Isolated DOX1 in mauve, and DOX2 in orange; (b) Isolated BNO-NS; (c) Comparison between DOX1 alone (mauve) and DOX1 in π−π interaction with BNO-NS (green); and (d) Comparison between DOX2 alone (blue) and chemisorbed on BNO-NS (in red).

4.2. Molecular dynamic simulations

MD simulations were used to study DOX1 physisorbed on BNO-NS and DOX2 chemisorbed on BNO-NS as isolated systems in a biological solvent, or as systems that interact with the cell membrane in a biological environment. The behavior of DOX1, DOX2 and BNO-NS alone was first analyzed with or without the cell membrane.

4.2.1. Isolated systems (without cell membrane).

First, all systems were stabilized and studied in water containing 0.15M NaCl (biological solvent). For DOX alone and BNO-NS alone, the root-mean-square deviation (RMSD) values did not show any important change because the variation ranged from 1.25 to 0.7 Å respectively, indicating a small deformation of the molecules.

Then, the DOX1/BNO-NS and DOX2/BNO-NS systems were progressively submitted to thermal agitation to study their stability. Like for isolated DOX and BNO-NS, the RMSD values of each system did not suggest any important variation of their backbone structure. A

maximum of 2.8 Å and of 2.5 Å were obtained for the DOX1/BNO-NS and for DOX2/BNO-NS system, respectively. These values were mainly explained by DOX deformation to land on the BNO-NS surface, which accounted for 60% of the total RMSD.

Once stabilized, the interaction energies of the molecules/systems with the solvent were extracted from the resulting trajectory (Table 2). The stability of each molecule alone (DOX and BNO-NS) in the solvent was very strong (-200 kcal/mol and -310 kcal/mol, respectively). Upon physical interaction (DOX1/BNO-NS), they lost part of their energy interaction with the solvent. As a consequence, the contribution of the interaction with the solvent was reduced to -150 (DOX1) and -220 kcal/mol (BNO-NS) for the physisorbed system (i.e., a total loss of -140 kcal/mol compared with DOX1 and BNO-NS alone). Although, they gained -100kcal/mol due to their mutual interaction, this was not sufficient to compensate the loss of interaction with the solvent. However, these numbers should be taken with caution due to the important deviations coming from the thermal agitation of the solvent. Indeed, the total energy for isolated DOX1 and BNO-NS oscillated between -490 and -530 kcal/mol, and between -410 and -530 kcal/mol for the physisorbed DOX1/BNO-NS system. The important fluctuations of the interaction energies coupled to a strong mutual pair interaction between DOX1 and BNO-NS explained the formation of the physisorbed system and its stabilization during the production runs (Table 2).

For the DOX2/BNO-NS system, the differential in terms of energy was clearly in favor of the isolated molecules. However, the MD simulations did not take into account bond formation or bond rupture between DOX2 and BNO-NS. Therefore, the system remained in its initial state, and the two molecules could not escape from each other. However, DOX2 position before and after the production run was drastically changed. At the beginning, a bond was created to place DOX2 perpendicularly to the BNO-NS surface (as obtained in DFT). During the simulations, DOX2 could rotate around its bond with BNO-NS and became positioned directly along the nanovector surface. This change of position allowed DOX2 to gain about -60 kcal/mol due to its interaction with the BNO-NS surface. This will have an important role in DOX2 transport to the membrane cell.

	DOX alone	BNO-NS alone	DOX1/BNO-NS	DOX2/BNO-NS

With solvent	-200 ± 10	-310 ± 10	-370 ± 60	-285 ± 25
Mutual interaction			-100 ± 10	-60 ± 10

Table 2: Pair interaction of isolated DOX or BNO-NS with the solvent (water + ions). For the DOX1 (or DOX2) system, the mutual interaction between DOX1 (DOX2) and BNO-NS was calculated.

4.2.2. Isolated molecules with the biological membrane

Before studying the influence of the BNO-NS nanovector on DOX interaction with the cell membrane, the diffusion of BNO-NS and DOX alone toward the lipid bilayer was analyzed. At the beginning of the simulation, the molecules were placed in the biological solvent (TIP3P water model with 0.15M NaCl) at about 25Å from the cell membrane surface (POPC).

	Isolated DOX	Isolated BNO-NS
With solvent	-200 ± 30	-180 ± 20
With POPC	40 ± 20	-195 ± 15

Table 3: Pair interactions of isolated DOX or BNO-NS with the biological solvent (water + ions) and with the cell membrane (constituted of POPC molecules). The calculations were performed when the BNO-NS was adsorbed on the cell membrane.

When BNO-NS was placed near the cell membrane, it first diffused randomly in the solvent before becoming strongly attracted by the membrane surface. BNO-NS moved very rapidly towards the membrane and landed flat on it, as indicated by the absolute average position of the flake compared with the cell membrane position (Fig. 5a). The interaction energy of BNO-NS in the solvent and once adsorbed on the membrane was clearly in favor of the adsorption on the membrane. Indeed, in the solvent, BNO-NS interaction energy with water was -310 kcal/mol, whereas on the cell membrane, the interaction came from the solvent (-180 kcal/mol) and also from the cell membrane (-195 kcal/mol) (Table 3). The loss of energy with the solvent was due to the presence of the cell membrane that prevented the solvent to completely surround the BNO-NS. This loss was compensated by the interaction with the cell

membrane surface that was more important than the solvent part (Fig. 5b).

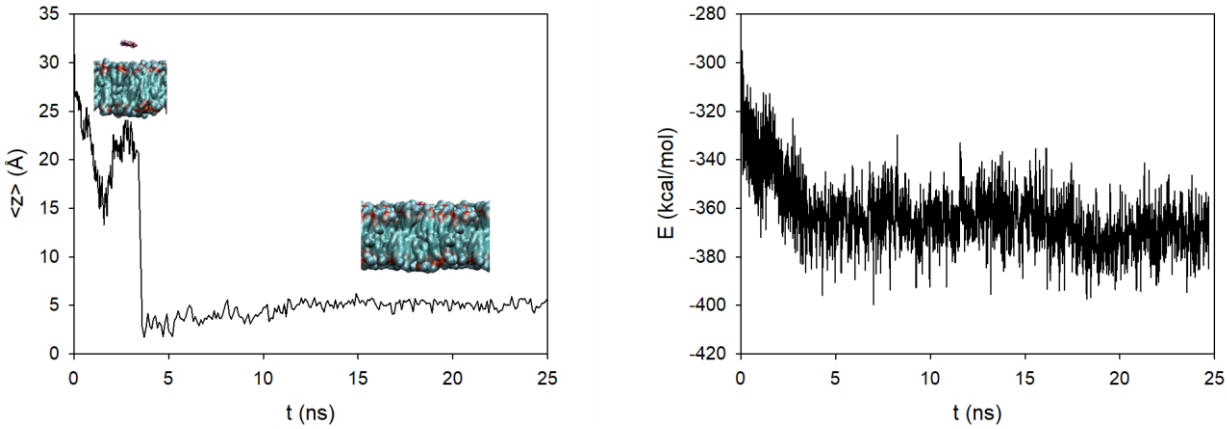

Figure 5: (a) Absolute average position (z) of BNO-NS relative to the cell membrane surface (positioned at z=0 Å) as a function of time. (b) Interaction energy (E, in kcal/mol) of BNO-NS in a box containing a POPC membrane as a function of time.

In figure add (a) and (b).

Conversely, when DOX was placed near a cell membrane, it randomly moved in the solvent box. It bounced off the cell membrane surface before returning to the solvent (Fig. 6a). The interaction energy between the membrane and DOX was in agreement with this observation (Fig. 6b). Indeed, in the solvent, DOX interaction energy with water was -200 kcal/mol. Near the cell membrane, the interaction energy with the membrane became positive (40 kcal/mol) (thus repulsive), while it was still negative with the solvent (Table 3). The strong repulsion between DOX and the cell membrane caused DOX displacement and made difficult its delivery to the cell membrane.

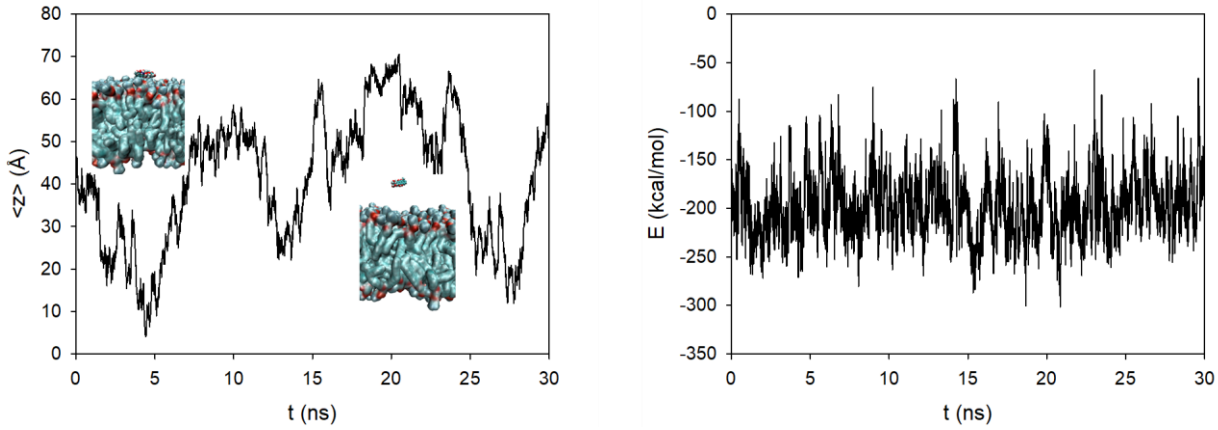

Figure 6: (a) Absolute average position (z) of DOX relative the cell membrane surface (positioned at z=0 Å) as a function of time. (b) Interaction energy (E, in kcal/mol) of DOX in a box containing a POPC membrane as a function of time.

In figure add (a) and (b).

4.2.3. The DOX1/BNO-NS and DOX2/BNO-NS systems with the biological membrane

The same simulation was performed for the anti-cancer drug physisorbed (DOX1) and chemisorbed (DOX2) on the BNO-NS nanovector. As before, the molecules were placed in the biological solvent containing the cell membrane at a distance of about 25Å, and were progressively heated to reach 310K. The relative trajectories of drug and nanovector, relative to the position of the cell membrane, showed the relative approach of the nanocargo towards the cell membrane (Fig. 7a). The DOX1/NBO-NS and DOX2/NBO-NS systems behaved in a completely different manner.

In the case of DOX1 physisorbed onto BNO-NS, the repulsive interaction between the drug and the cell membrane blocked its diffusion towards it. However, the strong affinity between the BNO-NS surface and the cell membrane forced the nanocargo (DOX1/BNO-NS) to diffuse quickly on the membrane (Fig. 7a). When the BNO-NS surface was in the good (optimal?) position (z=), the nanocargo could reach the cell membrane and did not leave it until the end of the simulation. DOX1/BNO-NS was adsorbed on the cell membrane with the drug molecule preferentially turned onto the cell. While strange, this position did not change until the end of the simulation.

DOX1/BNO-NS adsorption on the cell can be understood from the interaction energy of the

two molecules in the system. In water only, the total interaction of the DOX1/BNO-NS nanocargo with the solvent was -370 kcal/mol and DOX1 internal energy (mutual interaction) approached -100 kcal/mol (see Table 2). On the cell membrane, a small loss of energy was observed with the solvent due to BNO-NS positioning on the membrane cell (-320 kcal/mol), while the internal energy (mutual interaction) remained constant (-105 kcal/mol) (Table 4). On the contrary, the nanocargo interaction with the POPC surface accounted for -65 kcal/mol in the most favorable case (*i.e.*, when adsorbed on the surface). As a consequence, the difference of energy between DOX1/BNO-NS adsorbed on the cell membrane or free in the solvent was always favorable to the interaction with the cell membrane (around -20 kcal/mol). This means that, while the drug molecule alone was repulsed from the POPC surface, it could be transported and left on the cell membrane when adsorbed onto a BNO-NS. However, the small difference between the interaction energy in the POPC and in the solvent did not allow concluding on the true ability of BNO-NS to deliver the drug to its target.

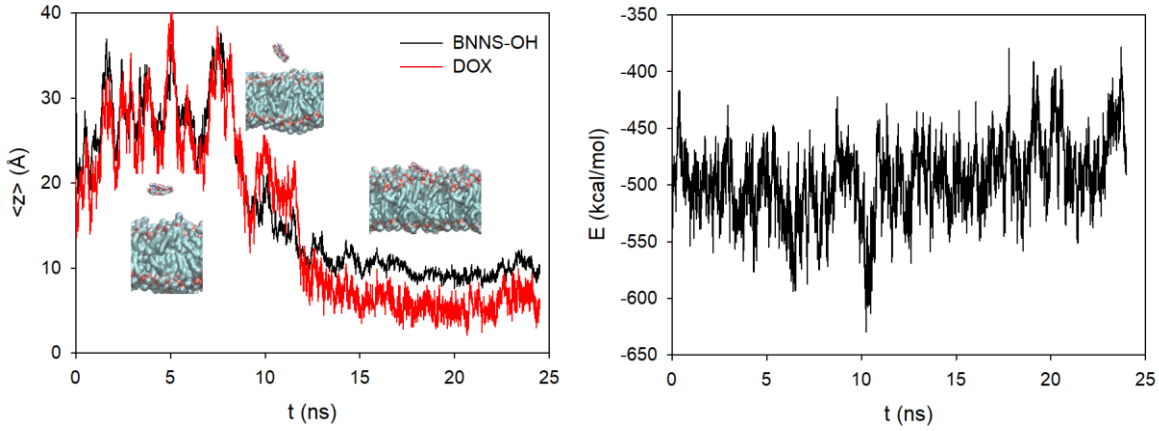

Figure 7: (a) Absolute average position of DOX1 physisorbed onto BNO-NS relative to the cell membrane surface (positioned at z=0 Å) as a function of time. (b) Interaction energy (in kcal/mol) of DOX1 physisorbed onto BNO-NS in a box containing a POPC membrane as a function of time.

In figure add (a) and (b).

	DOX1/NBO-NS	DOX2/NBO-NS
With solvent	-320 ± 20	-180 ± 20
With POPC	-65 ± 20	-145 ± 25

Mutual interaction	-105 ± 15	-55 ± 15

Table 4: Pair interaction of the DOX1/NBO-NS and DOX2/NBO-NS systems with the solvent (water + ions) and with the cell membrane (constituted of POPC molecules). The calculations were performed when the nanocargo was adsorbed on the cell. Mutual interaction corresponds to the direct DOX/BNO-NS interaction.

When DOX2 was chemisorbed on BNO-NS, the behavior of the system was very different. DOX2 was transported near the membrane in only 5ns (Fig. 8a). This quick diffusion can be explained by the important energy gain for DOX2 when interacting with the cell membrane (Fig. 8b). DOX2/BNO-NS total interaction energy was -345 kcal/mol in solvent, and -380 kcal/mol when close to the cell membrane (Table 4). In that case, the BNO-NS surface was flat on the cell membrane and the drug molecule landed on it. BNO-NS forced DOX2 to come close to the cell membrane, and thus filled its role as nanovector for a drug molecule that alone could not easily interact with the cell membrane.

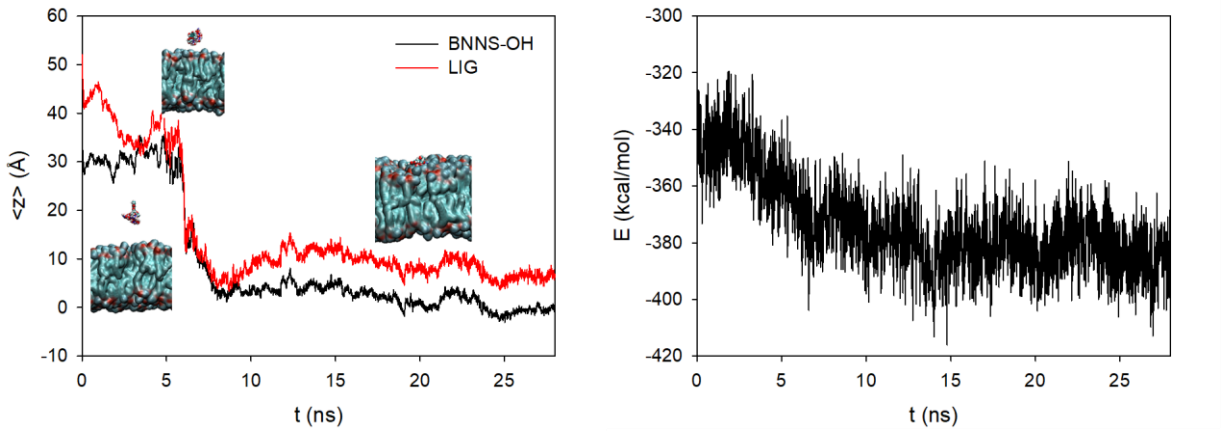

Figure 8: (a) Absolute average position (z) of the DOX2/NBO-NS system relative to the cell membrane surface (positioned at z=0 Å) as a function of time. (b) Interaction energy (E, in kcal/mol) of the DOX2/NBO-NS system in a box containing a POPC membrane as a function of time.

In figure add (a) and (b).

5. CONCLUSION

In this study, we investigated, using experimental data and DFT, TDDFT, and MD

simulations, the system involving DOX adsorbed on BNO-NS in environments of progressive complexity. Our results show that the non-covalent interactions of DOX on BNO-NS do not perturb its UV-vis response and its chemisorption. Therefore, DOX photodynamic response is not perturbed by the BNO-NS nanovector. Then, MD simulations were carried out to simulate a system close to the biological conditions. The MD results emphasize that the DOX/BNO-NS system remains energetically stable from water to a biological environment. The BNO-NS nanovector stabilized DOX close to the cell membrane. DOX UV-vis properties were not affected by interaction with BNO-NS, and DOX loading on BNO-NS could be determined theoretically and experimentally. In conclusion, hydrophilic BNO-NS loaded with DOX is a good candidate for the transport and stabilization of this anticancer compound near the cell membrane. While physisorption could be appropriate, chemisorption remains the best method to allow a good DOX delivery to its target. To the best of our knowledge, this is the first work using molecular dynamic simulations to show DOX/BNO-NS behavior near a cell membrane. All these results should reinforce the attention of the research community on BNO-NS for the delivery of therapeutic agents.

ACKNOWLEDGEMENTS

This present work was financially supported by University of Franche-Comté. Calculations were performed with the supercomputer regional facility Mesocenter of the University of Franche-Comté.

REFERENCES

[1] LaVan DA, McGuire T, Langer R. Small-scale systems for in vivo drug delivery. Nature Biotechnology 2003;21:1184-91.
[2] Jamieson T, Bakhshi R, Petrova D, Pocock R, Alexander M, Seifalian M. Biological applications of quantum dots. Biomaterials. 2007;28:4717-32.
[3] Wagstaff AJ, Brown SD, Holden MR, Craig GE, Plumb JA, Brown RE, et al. Cisplatin drug delivery using gold-coated iron oxide nanoparticles for enhanced tumour targeting with external magnetic fields. Inorganica Chimica Acta. 2012;393:328-33.
[4] Shi J, Kantoff PW, Wooster R, Farokhzad OC. Cancer nanomedicine: progress, challenges and opportunities. Nat Rev Cancer 2017;17:20–37.
[5] Chen H, Zhang W, Zhu G, Xie J, Chen X. Rethinking cancer nanotheranostics. Nat Rev Mater 2017;2:17024.
[6] Gu Y-J, Cheng J, Jin J, Cheng SH, Wong W-T. Development and evaluation of pH-responsive single-walled carbon nanotube-doxorubicin complexes in cancer cells. International Journal of Nanomedicine. 2011;6:2889-98.
[7] Kostarelos K, Bianco A, Prato M. Promises, facts and challenges for carbon nanotubes in imaging and therapeutics. Nat Nano. 2009;4(10):627-33.
[8] Liu Z, Tabakman S, Welsher K, Dai H. Carbon Nanotubes in Biology and Medicine: In vitro and in vivo Detection, Imaging and Drug Delivery. Nano Res. 2009;2(2):85-120.
[9] Weng Q, Wang X, Wang X, Bando Y, Golberg D. Functionalized hexagonal boron nitride nanomaterials: emerging properties and applications. Chem Soc Rev. 2016(45):3989-4012.
[10] Zhitnyak I, Bychkov I, Sukhorukova IV, Kovalskii AM, Firestein K, Golberg D, et al. Effect of BN Nanoparticles Loaded with Doxorubicin on Tumor Cells with Multiple Drug Resistance. ACS Applied Materials & Interfaces. 2017;9(38):32498-508.
[11] Khalifi ME, Bentin J, Duverger E, Gharbi T, Boulahdour H, Picaud F. Encapsulation capacity and natural payload delivery of an anticancer drug from boron nitride nanotube. Phys Chem Chem Phys. 2016;18(36):24994-5001.
[12] Nagarajan S, Belaid H, Pochat-Bohatier C, Teyssier C, Iatsunskyi I, Coy E, et al. Design of Boron Nitride/Gelatin Electrospun Nanofibers for Bone Tissue Engineering. ACS Applied Materials & Interfaces. 2017;9(39):33695-706.
[13] Ciesielski A, Samorì P. Graphene via sonication assisted liquid-phase exfoliation. Chem Soc Rev. 2014;43(1):381-98.
[14] Biscarat J, Bechelany M, Pochat-Bohatier C, Miele P. Graphene-like BN/gelatin nanobiocomposites for gas barrier applications. Nanoscale. 2015;7(2):613-8.
[15] Nasr M, Soussan L, Viter R, Eid C, Habchi R, Miele P, et al. High photodegradation and antibacterial activity of BN–Ag/TiO2 composite nanofibers under visible light. New Journal of Chemistry. 2018;42(2):1250-9.
[16] Golberg D, Bando Y, Huang Y, Terao T, Mitome M, Tang C, et al. Boron Nitride Nanotubes and Nanosheets. ACSNano. 2010;4(6):2979–93.
[17] Novoselov KS, Jiang D, Schedin F, Booth TJ, Khotkevich VV, Morozov SV, et al. Two-dimensional atomic crystals. PNAS. 2005;102(30):10451-3.
[18] Avouris P, Dimitrakopoulos C. Graphene: synthesis and applications. MaterialsToday. 2012;15(3):86-97.
[19] Tiano A, Park C, Lee J, Luong H, Gibbons L, Chu S, et al. Boron Nitride Nanotube: Synthesis and Applications. Nanosensors, Biosensors, and Info-Tech Sensors and Systems. 2014;9060:1-19.
[20] Chimene D, Alge DL, Gaharwar AK. Two-Dimensional Nanomaterials for Biomedical Applications: Emerging Trends and Future Prospects. Advanced Materials. 2015;27(45):7261-84.

[21] Weng Q, Wang B, Wang X, Hanagata N, Li X, Liu D, et al. Highly water-soluble, porous, and biocompatible boron nitrides for anticancer drug delivery. ACSnano. 2014;8(6):6123-30.
[22] Dreyer DR, Park S, Bielawski CW, Ruoff RS. The chemistry of graphene oxide Chemical Society Reviews. 2010;39:228-40.
[23] Sasidharan A, Panchakarla LS, Sadanandan AR, Ashokan A, Chandran P, Girish CM, et al. Hemocompatibility and macrophage response of pristine and functionalized graphene. Small. 2012;8 1251–63.
[24] Russier J, Treossi E, Scarsi A, Perrozzi F, Dumortier H, Ottaviano L, et al. Evidencing the mask effect of graphene oxide: a comparative study on primary human and murine phagocytic cells,. Nanoscale. 2013;5 11234–47.
[25] Messinger YH, Gaynon PS, Sposto R, Giessen Jvd, Eckroth E, Malvar J, et al. Bortezomib with chemotherapy is highly active in advanced B-precursor acute lymphoblastic leukemia: Therapeutic Advances in Childhood Leukemia & Lymphoma (TACL) Study. Blood. 2012;120(2):285-90.
[26] Tacar O, Sriamornsak P, Dass CR. Doxorubicin: an update on anticancer molecular action, toxicity and novel drug delivery systems. J Pharm Pharmacol. 2013;65(2):157-70.
[27] Du C, Zhao J, Fei J, Cui Y, Li J. Assembled Microcapsules by Doxorubicin and Polysaccharide as High Effective Anticancer Drug Carriers Adv Healthcare Mater 2013; 2(9):1246–51
[28] Mendes RG, Bachmatiuk A, Büchner B, Cuniberti G, Rümmeli MH. Carbon nanostructures as multi-functional drug delivery platforms J Mater Chem B. 2013(1):401-28.
[29] Ali-Boucetta H, Al-Jamal KT, McCarthy D, Prato M, Bianco A, Kostarelos K. Multiwalled carbon nanotube-doxorubicin supramolecular complexes for cancer therapeutics, . Chem Commun. 2008;0:459–61
[30] Gonzalez Ortiz D, Pochat-Bohatier C, Cambedouzou J, Balme S, Bechelany M, Miele P. Inverse Pickering Emulsion Stabilized by Exfoliated Hexagonal-Boron Nitride (h-BN). Langmuir. 2017;33(46):13394-400.
[31] Vidhyadevi T, Jules B, Jean-Marc J, Mikhael B, Maguy J, Sivanesan S, et al. Fluorescence Quenching of Sulfo-rhodamine Dye over Graphene Oxide and Boron Nitride Nanosheets. European Journal of Inorganic Chemistry. 2016;2016(13‐14):2125-30.
[32] Liao Y, Tu K, Han X, Hu L, Connell JW, Chen Z, et al. Oxidative Etching of Hexagonal Boron Nitride Toward Nanosheets with Defined Edges and Holes. Scientific Reports. 2015;5:14510-12.
[33] Lin Y, Williams TV, Xu T-B, Cao W, Elsayed-Ali HE, Connell JW. Aqueous Dispersions of Few-Layered and Monolayered Hexagonal Boron Nitride Nanosheets from Sonication-Assisted Hydrolysis: Critical Role of Water. J Phys Chem C. 2011;115(6):2679–85.
[34] Kumar V, Nikhil K, Roy P, Lahiri D, Lahiri I. Emergence of fluorescence in boron nitride nanoflakes and its application in bioimaging RSC Adv. 2016;6(53):48025-32.
[35] Hohenberg P, Kohn W. Inhomogeneous Electron Gas. Phys Rev. 1964;136(3B):864-71.
[36] Kohn W, Sham LJ. Self-Consistent Equations Including Exchange and Correlation Effects. Phys Rev. 1965;140(4A):1133-8.
[37] Perdew JP, Burke K, Ernzerhof M. Generalized Gradient Approximation Made Simple. Phys Rev Lett 1996;77:3865-8.
[38] Ordejon P, Artacho E, Soler JM. Self-consistent order-N density-functional calculations for very large systems. Phys Rev B 1996;53:10441-4.

[39] Sainsbury T, Satti A, May P, Wang Z, McGovern I, Gun'ko YK, et al. Oxygen Radical Functionalization of Boron Nitride Nanosheets. J Am Chem Soc. 2012;134(45):18758-71.
[40] Lee D, Lee B, Park KH, Ryu HJ, Jeon S, Hong SH. Scalable Exfoliation Process for Highly Soluble Boron Nitride Nanoplatelets by Hydroxide Assisted Ball Milling. Nano Lett. 2015;15(2):1238−44.
[41] Lin Y, Williams TV, Connell JW. Soluble, Exfoliated Hexagonal Boron Nitride Nanosheets. J Phys Chem Lett. 2010 1(1):277−83.
[42] Weng Q, Wang B, Wang X, Hanagata N, Li X, Liu D, et al. Highly Water-Soluble, Porous, and Biocompatible Boron Nitrides for Anticancer Drug Delivery. ACS Nano. 2014;8(6):6123-30.
[43] Bader RFW. A Quantum Theory of Molecular Structure and its Applications. Chem Rev 1991;91(5):893-928.
[44] Henkelman G, Arnaldsson A, Jońsson H. A fast and robust algorithm for Bader decomposition of charge density. Comput Mater Sci 2006;36(3):354-60.
[45] Andrade X, Strubbe D, Giovannini UD, Larsen AH, Oliveira MJT, Alberdi-Rodriguez J, et al. Real-space Grids and the Octopus Code as Tools for the Development of New Simulation Approaches for Electronic Systems. Phys Chem Chem Phys. 2015;17(47):31371−96.
[46] Castro A, Appel H, Oliveira M, Rozzi CA, Andrade X, Lorenzen F, et al. Octopus: a Tool for the Application of Time-dependent Density Functional Theory. Phys Status Solidi B. 2006;243(11):2465−88.
[47] Marques MAL, Castro A, Bertsch GF, Rubio A. Octopus: a First-principles Tool for Excited Electron-ion Dynamics. Comput Phys Commun. 2003;151(1):60−78.
[48] Mayne CG, Saam J, Schulten K, Tajkhorshid E, Gumbart JC. Rapid Parameterization of Small Molecules Using the Force Field Toolkit. J Comput Chem. 2013;34(32):2757−70.
[49] Jo S, Kim T, Iyer VG, Im W. CHARMM-GUI: a Web- based Graphical User Interface for CHARMM. J Comput Chem. 2008;29(11):1859−65.
[50] Best RB, Zhu X, Shim J, Lopes PEM, Mittal J, Feig M, et al. Optimization of the Additive CHARMM All- Atom Protein Force Field Targeting Improved Sampling of the Backbone φ, ψ and Side-Chain χ1 and χ2 Dihedral Angles. J Chem Theory Comput. 2012;8(9):3257−73.
[51] Mauro N, Campora S, Scialabba C, Adamo G, Licciardi M, Ghersi G, et al. Self-organized environment-sensitive inulin– doxorubicin conjugate with a selective cytotoxic effect towards cancer cells. RSC Adv. 2015;5:32421-30.